Targeting the right metrics for an efficient solvent-free formulation of PEO:LiTFSI:Li6PS5Cl hybrid solid electrolyte

Ronan Chometon, Michaël Deschamps, Romain Dugas, Elisa Quemin, Benjamin Hennequart, Marc Deschamps, Jean-Marie Tarascon, Christel Laberty-Robert

Targeting the right metrics for an efficient solvent-free formulation of PEO:LiTFSI:Li_6PS_5Cl hybrid solid electrolyte

Ronan Chometon[1,2,3,5], Michaël Deschamps[4,5], Romain Dugas[1,5], Elisa Quemin[1,5], Benjamin Hennequart[1,5], Marc Deschamps[3], Jean-Marie Tarascon[1,5] and Christel Laberty-Robert[2,5] *

1. Collège de France, Chaire de Chimie du Solide et de l'Energie, UMR8260, 11 place Marcelin Berthelot, 75231 Paris Cedex 05, France
2. Sorbonne Université, Laboratoire de Chimie de la Matière Condensée, UMR7574, 4 place Jussieu, 75005 Paris, France
3. Blue Solutions, Odet, 29500 Ergué-Gabéric, France
4. CNRS-CEMHTI, UPR3079, Université d'Orléans, 1D avenue de la Recherche Scientifique, Orléans Cedex, 45071 France
5. Réseau sur le Stockage Électrochimique de l'Energie (RS2E), FR CNRS 3459, 80039 Amiens, France

* Corresponding Author (christel.laberty@sorbonne-universite.fr)

KEYWORDS

solid-state battery, hybrid solid electrolyte, argyrodite, polymer electrolyte, organic-inorganic interphase, Arrhenius, VFT

ABSTRACT

Hybrid solid electrolytes (HSEs) aim at combining the superior ionic conductivity of inorganic fillers with the scalable process of polymer electrolytes in a unique material for solid-state batteries. Pursuing the goal of optimizing the key metrics ($\sigma_{ion} \geq 10^{-4}$ S.cm^{-1} at 25°C and self-standing property), we successfully developed a HSE based on a modified poly(ethylene oxide):LiTFSI organic matrix which binds together a high loading (75 wt.%) of Li_6PS_5Cl particles, following a solvent-free route. A rational study of available formulation parameters has enabled us to understand the role of each component in the conductivity, the mixing and the mechanical cohesion. Especially, the type of activation mechanism (Arrhenius or Vogel-Fulcher-Tammann (VFT)) and its associated energy are proposed as a new metric to unravel

the ionic pathway inside the HSE. We showed that a *polymer-in-ceramic* approach is mandatory to obtain enhanced conduction through the HSE ceramic network, as well as superior mechanical properties, revealed by tensile test. Probing the compatibility of phases, using electrochemical impedance spectroscopy (EIS) alongside ^{7}Li nuclear magnetic resonance (NMR), reveals the formation of an interphase, the quantity and resistivity of which grow with time and temperature. Finally, electrochemical performances are evaluated by assembling a HSE-based battery, which displays comparable stability as pure-ceramic ones but still suffers from higher polarization and thus lower capacity. Altogether, we hope these findings provide valuable knowledge to develop a successful HSE, by placing the optimization of the right metrics at the core of the formulation.

INTRODUCTION

Solid-state batteries (SSBs) generate immense excitement as a potential upgrade to Li-ion technology, offering the promise of higher energy density and enhanced safety. The key to this technology lies in the use of lithium metal as the anode, leading to a theoretical increase of 70% in volumetric ($Wh.L^{-1}$) and 40% in gravimetric ($Wh.kg^{-1}$) energy densities[1]. Recent advancements in the development of solid inorganic ionic conductors, such as $Li_{10}GeP_2S_{12}$ in 2011 (10^{-2} $S.cm^{-1}$)[2] and argyrodite - Li_6PS_5X, X = Cl, Br, I - in 2008 (10^{-3} $S.cm^{-1}$)[3], have demonstrated conductivity comparable to that of liquid electrolytes. However, it is important not to overlook their inherent limitations. Ceramic electrolytes are brittle materials: they require high pressure during cell assembly and when cycling, to ensure sufficient contact between particles and limit cracks appearance.[4] They cannot therefore be directly implemented in commercial cells, as pure-ceramic processing would require an entirely new design of existing Li-ion batteries (LIB) manufacturing lines. The need for flexible, easily processable solid electrolytes makes hybrid solid electrolytes (HSEs) a tangible compromise to get mechanical stability along with sufficient ionic conductivity. They are typically composed of inorganic particles embedded in a polymer electrolyte phase. The addition of these particles serves a dual purpose: to enhance the room temperature ionic conductivity and to reinforce the organic phase. In fact, polymer electrolytes suffer from low ionic conductivity at room temperature (10^{-7} to 10^{-5} $S.cm^{-1}$)[5] but stand out for their mechanical properties and ease of processing. Poly(ethylene oxide) (PEO) combined with a dissolved lithium salt is the system dominating the field since its discovery by Wright in 1973[6] and its first application in a battery

proposed by Armand in 1978[7]. When used above its melting point, which is its current commercial application[8], its conductivity becomes sufficient to cycle a battery, but mechanical integrity must be ensured by another polymer (e.g. PVDF-HFP)[9]. With the aim to increase room temperature conductivity, the addition of non-conductive inorganic nanoparticles, such as Al_2O_3[10], SiO_2[11] or TiO_2[11,12], results in the suppression of polymer crystalized domains, which reinforces the segmental mobility of Li^+ along polymer chains. Additionally, the Lewis acid property of these fillers favors the dissociation of the lithium salt. Altogether, those properties increases the HSE ionic conductivity at room temperature.

More recently, conductive inorganic particles have been incorporated into a polymer matrix to develop new types of HSE. Ceramic electrolytes, whether oxides (e.g. LLZO[13–15]) or sulfides (e.g. LGPS[16,17], Li_3PS_4[18], Li_6PS_5Cl[19,20]) have been extensively studied, each time in combination with different types of polymer electrolytes. Two different approaches emerge from the literature[21]: (i) the addition of a small amount of ceramic filler to disturb the crystallinity of the organic phase, known as a *ceramic-in-polymer* system; (ii) and its opposite, in which the polymer electrolyte, in low content, acts primarily as a binder, called *polymer-in-ceramic*. Overall, the wide range of reported formulations often leads to a large disparity of performances.[22] The formulation of a HSE requires fine tuning of the available parameters: polymer chemistry and molecular weight, choice of Li salt anion and concentration, type of ceramic electrolyte (particle size, surface chemistry), organic-to-inorganic ratio, presence of plasticizer and mixing route (wet or dry). Most published work on sulfide HSEs introduce slurry-assisted preparation, which outperforms dry mixing in terms of homogeneity and ease of processing. However, the wet process suffers from the instability of the ceramic towards the solvent[23,24] and the extensive coverage of the particles by the binder, which impedes lithium ion transfer[25,26]. The practical metrics, that should guide the design of an effective HSE, are its ionic conductivity and mechanical properties. To guarantee the cyclability of a HSE-based battery, 10^{-4} $S.cm^{-1}$ is required at room temperature with a self-standing property and a thickness of 10 µm to achieve an ohmic drop similar to that of a typical Li_6PS_5Cl separator (350 µm and 3 $mS.cm^{-1}$). In the perspective of formulating the best HSE, it is also essential to understand possible reactivity at the interface between organic and inorganic phases to assess the extent to which it may be detrimental.

In this study, we propose a rational solvent-free formulation of a HSE based on PEO and LiTFSI (Lithium bis(trifluoromethanesulfonyl)imide) as the organic electrolyte and Li_6PS_5Cl argyrodite as ceramic phase. With the aim of meeting the two criteria of conductivity at room temperature (10^{-4} S.cm^{-1} at 25°C) and self-standing property, we explore various adjustable parameters: Li salt concentration, organic-to-inorganic ratio and polymer molar mass. We unravel a ceramic content threshold above which we observed a change in conductivity and mechanical properties, leading to a necessary compromise. After successfully reaching this threshold by fine-tuning of the PEO molar mass, we characterize the mechanical properties of the optimized HSE and provide insight into the interphase, by electrochemical impedance spectroscopy (EIS) and nuclear magnetic resonance (NMR). Finally, we probe the practical assets of our HSE by testing its electrochemical performances in a full-cell SSB and demonstrate its good capacity retention.

EXPERIMENTAL SECTION

Materials and electrolytes preparation

Preparation of electrolytes was carried out in an argon-filled glovebox (O_2 < 1 ppm and H_2O < 1 ppm). PEO of different molar mass (600, 6 and 1.5 kg.mol^{-1}) were bought from Sigma-Aldrich and dried just below their respective melting point under vacuum for two days. The same procedure was applied to poly(ethylene-co-propylene oxide) (P(EO-co-PO), Meisei Chemical Works, Ltd.). Poly(ethylene glycol) (PEG 0.4 kg.mol^{-1}) was dried over molecular sieves (4Å) inside the glovebox. LiTFSI from Solvionic was vacuum dried at 110°C for two days. The ceramic solid electrolyte Li_6PS_5Cl was purchased from NEI Corporation (d ≈ 1 - 30 µm). The NMC cathode active material ($LiNi_{0.6}Mn_{0.2}Co_{0.2}O_2$ monolithic, d ≈ 4 µm) was kindly provided by UMICORE. Vapor Grown Carbon Fibers (VGCF) were bought from Sigma-Aldrich and dried at 280°C under vacuum for one day. Polyvinylidene Fluoride-Hexafluoropropylene (PVDF-HFP) binder was obtained from Solvay.

HSEs were prepared following a dry mixing of powders in an agate mortar. First, LiTFSI was mixed with the desired quantity of polymer and the resulting gum was hot pressed (80°C) several times between poly(ethylene terephthalate) (PET) foils to ensure homogeneity. Then, the appropriate amount of Li_6PS_5Cl powder was grinded for 5 min and the organic phase was added to Li_6PS_5Cl to agglomerate. The obtained HSE paste was spread as a thin membrane (e

≈ 100 µm) by hand-rolling it between PET foils. In case the membrane processing was not possible due to lack of mechanical cohesion, the HSE was pelletized in an 8 mm diameter die-set under 100 MPa for 1 min, using a manual hydraulic press (Specac, 15T).

The organic-to-inorganic ratio is expressed in both mass and volume according to the following equation:

$$x_{inorg}^{V} = \frac{x_{inorg}^{M}}{x_{inorg}^{M} + \left(1 - x_{inorg}^{M}\right) \cdot \frac{\rho_{inorg}}{\rho_{org}}} \quad \textbf{Equation 1}$$

where x_{inorg}^{V} (resp. x_{inorg}^{M}) is the volume (resp. mass) fraction of the inorganic phase, ρ_{inorg} = 1.64 g.cm^{-3} is Li_6PS_5Cl theoretical density and ρ_{org} = 1.4 g.cm^{-3} is the organic phase density. ρ_{org} is calculated according the following equation:

$$\rho_{PEO:LiTFSI} = \rho_{PEO} \cdot \frac{1 + A}{\frac{\rho_{PEO}}{\rho_{LiTFSI}} + A} \quad \textbf{Equation 2}$$

where ρ_{PEO} ≈ 1.2 g.cm^{-3}, ρ_{LiTFSI} = 2.023 g.cm^{-3} and $A = EO{:}\,Li \cdot \frac{M_{EO} \cdot M_{PEO}}{(M_{PEO} - M_{H_2O}) \cdot M_{LiTFSI}}$ (**Equation 3**).

The ratio of lithium in the organic phase is expressed as

$$R_{org}^{Li} = \frac{n_{org}^{Li}}{n_{org}^{Li} + n_{inorg}^{Li}} = \frac{x_{org}^{V} \cdot C_{org}^{Li}}{x_{org}^{V} \cdot C_{org}^{Li} + x_{inorg}^{V} \cdot C_{inorg}^{Li}} \quad \textbf{Equation 4}$$

where $C_{org}^{Li} = \left(\frac{M_{LiTFSI}}{\rho_{LiTFSI}} + EO{:}\,Li \cdot \frac{M_{EO}}{\rho_{PEO}}\right)^{-1}$ = 1.9 mmol.cm^{-3} (**Equation 5**) and C_{inorg}^{Li} = 36.7 mmol.cm^{-3}.[27]

Ionic conductivity measurements

According to a blocking electrode configuration, polymer electrolytes and HSEs were placed between stainless steel discs and Li_6PS_5Cl pellets were faced with carbon electrodes to ensure good contact. A dedicated two-electrode cell (Fig. S15a), developed in our laboratory, was employed to perform EIS measurements. It is composed of a body in three parts (PEI and stainless steel) that are assembled together with screws. The HSE membrane, wider than the cell section (0.5027 cm^2), was clamped in between these parts before placing the stainless steel discs. The cell was then closed with the stainless steel plungers using dedicated screws at a constant torque of 1.7 N.m. Airtightness was ensured by compressed O-rings. The cells

were preheated at 80°C for 1h in advance of the measurement to improve the contact between electrodes and electrolyte. EIS was performed in the frequency range of 1 MHz – 1 Hz with a voltage amplitude of 50 mV, using a VMP3 potenstiotat/galvanostat (BioLogic) controlled by EC-lab® software. Fifteen points were acquired per decade of frequency with ten repetitions per point. To determine activation mechanism and the associated energy (Arrhenius or VFT), temperature was applied to the cell through heated silicon oil traveling in a PVC pipe wrapped around the cell. It was connected to a thermal immersion circulator (ThermoFisher Scientific), controlled by EC-lab® to vary the temperature from 20 to 80°C, with step of 20°C and 3h intervals for equilibration. In parallel, real cell temperature was monitored thanks to a thermocouple inserted in the upper cell plunger, for sake of precision when calculating activation energies. Conductivities were calculated with the following equation:

$$\sigma_{ionic} = \frac{e}{S \cdot R_{ionic}} \qquad \textbf{Equation 6}$$

where e is the membrane thickness, S the cell section and R_{ionic} the ionic resistance by reading the real impedance value at the high-frequency intercept of the arc onto the Nyquist diagram.

Scanning electron microscopy

HSE cross section morphology was observed on a FEI Magellan scanning electron microscope (SEM) and samples were prepared by blade cutting inside glovebox.

Differential scanning calorimetry

Thermal properties of the prepared electrolytes were studied with a differential scanning calorimeter (DSC – TA Instruments Q20) in the temperature range of -70 – 200°C, at a heating rate of 10 °C.min^{-1}. Samples of 5 – 15 mg were hermetically sealed in aluminum pans inside the argon-filled glovebox. Analysis of the melting enthalpy allows the calculation of the degree of crystallinity for PEO_x:LiTFSI electrolytes:

$$\chi_c = \frac{\Delta H^{melt}_{PEO\ in\ electrolyte}}{\Delta H^{melt}_{pure\ PEO}} \qquad \textbf{Equation 7}$$

Mechanical characterization

Tensile test was performed on a universal testing machine (Zwick Z100) located in a dry room (dew point below - 40°C). HSE paste was first calendered as a large-area membrane (e = 100

µm) thanks to a prototyping machine. Four samples per formulation were cut to the chosen dimensions (60 x 10 mm), fixed at a distance of 41 mm between jaws and tested at a load rate of 5 mm.min^{-1}. Force was measured against the elongation until the sample fractures (F = 0 N) and the stress-strain curve ($\sigma - \varepsilon$) is obtained using these equations:

$$\sigma = \frac{F}{S} \; ; \text{in } MPa \qquad \textbf{Equation 8}$$

$$\varepsilon = \frac{\Delta L}{L_0} \; ; \text{in } \% \qquad \textbf{Equation 9}$$

$$E = \frac{\sigma}{\varepsilon} \; ; \text{in } MPa \qquad \textbf{Equation 10}$$

with F the force, S the sample section, ΔL the elongation and L_0 the initial distance between jaws. Young's modulus E is calculated by fitting the initial linear domain (ε = 1.22% for HSE 40 wt.% ceramic and ε = 0.14 % for HSE 75 wt.% ceramic). Yield strength σ_y is the stress at the end of the linear (i.e. elastic) limit. Ultimate strength σ_u is defined as the maximum of stress undergone by the sample. Resilience modulus U_r is calculated as the elastic energy (area under the stress-strain curve in the linear domain) and toughness modulus U_t is computed as the total energy absorbed before fracturing.

$$U_r = \frac{\sigma_y^2}{2E} \; ; \text{in } J.m^{-3} \qquad \textbf{Equation 11}$$

$$U_t = \int_0^{\varepsilon_f} \sigma \cdot d\varepsilon \; ; \text{in } J.m^{-3} \qquad \textbf{Equation 12}$$

EIS to determine interfacial resistance

To measure the interfacial resistance between the organic and inorganic phases, trilayer stack of PEO_x:LiTFSI | Li_6PS_5Cl | PEO_x:LiTFSI were assembled (x = 10, 20 and 40). Polymer electrolyte membranes were prepared by hot pressing (80°C) between PET foils to reach a thickness of 35 µm. Ceramic powder was densified as a pellet at 400 MPa using an 8 mm diameter die-set. Then, polymer membranes were carefully attached to the cell stainless steel plungers and the ceramic pellet was place in between them before closing. A pressure of 4.5 MPa was applied *via* a spring assisted setup, so that the polymer does not creep at high temperature. EIS was performed at room temperature before and after an hour stabilization at 80°C. Afterwards, temperature-dependent EIS was carried out in the same conditions as previously described. Impedance data were fitted with Z-view4 software (Scribner). The following model (Scheme 1) was used to extract R_{ionic} and $R_{interface}$:

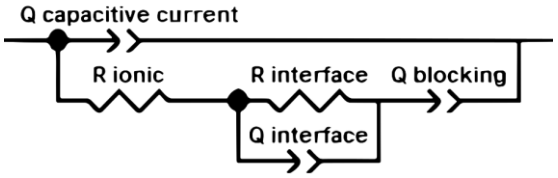

Scheme 1

with R_{ionic} the resistance of electrolytes, $R_{interface}$ and $Q_{interface}$ the contribution of the interface and $Q_{blocking}$ describing the capacitive response against blocking electrodes at low frequency. The other branch, composed only of $Q_{capacitive\ current}$, describes the capacitive current in parallel to the faradic current.

X-ray photoelectron spectroscopy

XPS spectra were collected on an Omicron Argus X-ray photoelectron spectrometer, using a monochromated Al Kα (hν = 1486.6 eV) radiation source having a 300 W electron beam power. The samples were analyzed under ultra-high vacuum conditions (1 x 10^{-8} Pa). After recording a broad range spectrum (pass energy 100 eV), high resolution spectra were recorded for all core XPS levels (Pass energy 20 eV). Spectrum processing was carried out using the Casa XPS software package. The spectra were fitted by applying a Gaussian/ Lorentzian function with a ratio G/L equal to 70:30.

Nuclear magnetic resonance

^{7}Li NMR spectra were recorded on a 20T (850 MHz for ^{1}H, 330 MHz for ^{7}Li) Bruker WB Avance spectrometer equipped with 1.3 mm ^{1}H-^{19}F/X double resonance probe head. The Magic Angle Sinning (MAS) rate was set at 40 kHz to prevent unwanted pressure gradients on the polymer sample inside the ZrO_2 rotor, and the bearing and drive gas were pure nitrogen. The samples were prepared inside an argon-filled glovebox. The ^{7}Li chemical shift was referenced with 1M ^{7}LiCl in water, and the RF strength was set to 86 kHz (90° pulse of 2.9 µs). The longitudinal relaxation times of ^{7}Li in argyrodite and the polymer phase were measured in the same conditions at 526 ms and 1.0 s respectively. All 1D spectra were recorded using a rotor synchronized Hahn echo sequence (with a half echo time equal to a single rotor period), using a recovery delay of 5 s to ensure quantitative measurements, and 16 transients were recorded for each. The EXchange SpectroscopY 2D experiment was recorded with a 1.5 s recovery delay, 64 transients were recorded for each one of the 512 time increments, and the sweep width in the indirect dimension was set to 2000 Hz, using the States method for quadrature detection.

Battery assembly and electrochemical testing

Battery assembly and electrochemical tests were carried out in the same cell (Fig. S15a) as for ionic conductivity measurement, when HSE was used as the separator. When a pellet of Li_6PS_5Cl fulfilled this task, we used a simpler version of our two-electrode cell (Fig. S15b), consisting in a unique PEI body and two stainless steel plungers. The assembly followed a first step of placing the electrolyte: either by clamping a HSE membrane (e ≈ 100 µm) or by compressing 30 mg of Li_6PS_5Cl (e ≈ 400 µm) in the cell body at 100 MPa for few seconds, thanks to a manual hydraulic press. The next steps were identical for both battery configurations. A disc of cathode was placed on one side (m ≈ 4 mg – e ≈ 30 µm) and the appropriate amount of counter electrode powder ($Li_{0.5}In$: Li_6PS_5Cl = 60:40 (w)) was spread on the other side (m ≈ 30 mg – e ≈ 250 µm). The whole stack was finally densified under 400 MPa for 15 min (e_{tot} ≈ 700 µm). The closure was carried out by applying 2.3 N.m to each screw to obtain an internal pressure of 100 MPa. All assembly steps were performed in an argon-filled glovebox to prevent any potential contamination from moisture. Cathode tape was prepared by hand-grinding powders in an agate mortar to reach the desired ratio NMC622 : Li_6PS_5Cl : VGCF = 67.2 : 28.8 : 1.5 (w). 2.5 wt.% of PVDF-HFP was then added to the mix. To prepare the slurry, powders and the appropriate amount of ethyl acetate (extra dry 99.9%, Thermo Scientific) were stirred together for 15 min. It was then casted onto the aluminum current collector using the doctor blade method and tape was vacuum dried at 60°C for 12h.

Galvanostatic cycling was performed in the voltage range of 2.1 – 3.6 V vs LiIn/In (2.72 – 4.22 V vs Li^+/Li) at a varying C-rate (calculated according to theoretical capacity Q_{NMC622} = 276.5 $mAh.g^{-1}$): two cycles at C/20 followed by five cycles steps of C/10, C/5, C/2 and C before long cycling at C/5. Measurements were conducted on a BCS potentiostat/galvanostat (BioLogic) controlled with EC-Lab® software.

RESULTS AND DISCUSSION

Salt concentration in organic phase

The organic phase for preparing HSE was formulated in order to maximize its ionic conductivity at room temperature. In the model system of PEO:LiTFSI, salt concentration (or inversely EO:Li ratio) is the key parameter to adjust both Li^+ conductivity and mechanical properties.[28–30] In accordance with literature, the EO:Li = 10 ratio was chosen because of its high room

temperature conductivity. Measured by EIS in a blocking electrode configuration, it reaches 2.10^{-5} S.cm^{-1} at 20°C compared with the less concentrated electrolyte (EO:Li = 20), which displays only 5.10^{-6} S.cm^{-1} (Fig. S1a). This increase of conductivity, occurring below the melting temperature of PEO (T_m = 40-55.9 °C depending on the salt concentration), is due to the shrinkage of pure PEO crystalline domains which are not Li^+ conductive, as illustrated by the decrease in enthalpy of fusion measured by DSC at high salt concentration (Fig. S1b). Consequently, we choose the highly concentrated polymer electrolyte (EO:Li = 10) as the organic phase for HSE formulation.

Organic-to-inorganic ratio

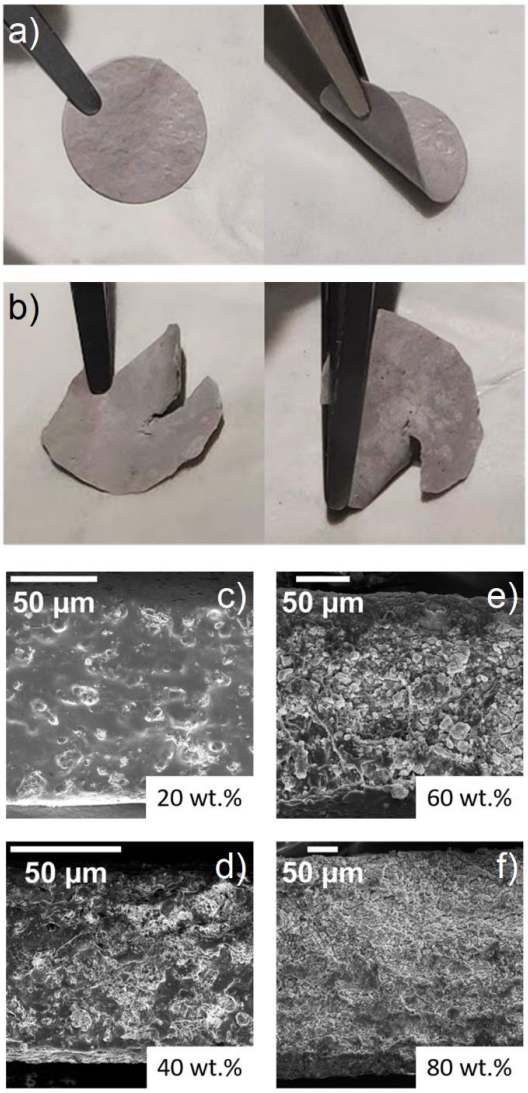

Figure 1: Influence of organic-to-inorganic ratio on HSE preparation. Images of (a) flexible HSE (60 wt.% Li_6PS_5Cl) and (b) brittle HSE (80 wt.% Li_6PS_5Cl). (c) to (f) SEM cross-section pictures of HSE according to the ceramic content.

HSEs composed of PEO_{10}:LiTFSI (also indistinctly referred as polymer phase or organic phase) and Li_6PS_5Cl (also indistinctly referred as ceramic phase or inorganic phase) were prepared varying the inorganic mass ratio from 20 to 95 % by weight. The precursors were dry mixed in a mortar, to avoid possible reactivity between Li_6PS_5Cl and a solvent, then hand spread to form a membrane when possible (see the Experimental section). The mechanical properties of the films obtained differ according to the quantity of ceramic particles. HSEs with an inorganic content of 60 wt.% or less are flexible, self-supporting membranes (Fig. 1a), while HSEs with more than 75wt.% Li_6PS_5Cl are difficult to agglomerate and the resulting material is brittle (Fig. 1b). Depending on the ratio, the prepared membranes exhibit mechanical behavior similar to either polymer (≤ 60 wt.% ceramic) or a ceramic (≥ 75 wt.%). SEM images of HSE cross-sections (Fig. 1c-f) show a globally homogeneous distribution of ceramic particles within the polymer electrolyte matrix. However, due to Li_6PS_5Cl particle sizes ranging from 1 to 30 µm (Fig. S2), the membranes are heterogeneous at the micrometer level, resulting in increased roughness for HSEs with high inorganic content.

Figure 2a shows the effect of the organic-to-inorganic ratio on ionic conductivity of HSE, at temperatures ranging from 20 to 80°C. There is no noticeable effect of adding ceramics to the polymer electrolyte up to 75 wt.% at each temperature step. In contrast, the addition of a small amount of PEO_{10}:LiTFSI (from 5 to 20 wt.%) to the ceramic powder results in a significant decrease in the ionic conductivity of the HSE, with a similar trend at each temperature. The threshold at which conductivity starts to increase, around 75 wt.% of ceramic, corresponds well to the transition from a flexible, self-standing membrane to a brittle mixture. This implies that a compromise between mechanical and conductivity properties will be necessary to meet the expected HSE requirements. Figure 2b shows the ionic conductivities as a function of temperature and the associated mechanism for the precursor materials and two selected HSEs. Li_6PS_5Cl can be fitted according to an Arrhenius model[31] (Equation 13) with an activation energy E_a of 0.41 eV, in good agreement with Hanghofer et al.[32] who reported a value of 0.396 eV.

$$\sigma = \frac{\sigma_0}{T} \cdot \exp\left(-\frac{E_a}{k \cdot T}\right) \qquad \textbf{Equation 13}$$

PEO_{10}:LiTFSI exhibits a different type of temperature activation due to the segmental mobility of the polymer chains. Conductivity follows the empirical Vogel-Fulcher-Tammann (VFT) [33–35]

model (Equation 14), which describes the conduction in amorphous electrolytes above the glass transition temperature T_g. σ_0 is the pre-exponential factor, k the Boltzmann constant, B the pseudo-activation energy and T_0 the Vogel temperature. The latter is equal to the glass transition in ideal glasses but is generally set 50°C below T_g for salt-in-polymer complexes.[31,36]

$$\sigma = \frac{\sigma_0}{T} \cdot \exp\left(-\frac{B}{k \cdot (T - T_0)}\right) \qquad \textbf{Equation 14}$$

For HSEs, the model that best describes their activation mechanism was chosen based on the highest value of the adapted correlation coefficient between VFT and Arrhenius fits (Fig. S3 and S4). This again corresponds to the two domains of the organic-to-inorganic ratio: HSEs with ≤ 60 wt.% of ceramic behaves like PEO_{10}:LiTFSI following a VFT model, while HSEs with ≥ 75 wt.% follow an Arrhenius law similar to Li_6PS_5Cl (Fig. 2c). The addition of ceramic particles (from 20 to 60 wt.%) to the organic matrix has no significant effect on the pseudo-activation energy B which remains stable around 0.11 eV (Fig. 2c), in the same way as conductivity. Clearly, the absence of PEO crystalline domains in the starting polymer phase (Fig. S1) makes the presence of inorganic fillers insignificant, as long as organic phase percolation is maintained (< 30 vol.%)[37]. To confirm this, we prepared a HSE without LiTFSI to suppress the conductivity of the organic phase (Fig. S5), with 50 vol.% of Li_6PS_5Cl. The resulting HSE conductivity ($1.4 \cdot 10^{-6}$ S.cm^{-1}) is ten times lower than the one containing LiTFSI (56 vol.% of Li_6PS_5Cl). In the absence of LiTFSI, the ionic pathway must occur through the network of Li_6PS_5Cl which is very tortuous and thus, impeded by non-conductive PEO. With LiTFSI, the organic network can conduct Li ions faster than Li_6PS_5Cl tortuous network. Following a *polymer-in-ceramic* approach, the addition of a small amount of organic phase (from 5 to 25 wt.%) results in a higher activation energy (from 0.49 to 0.69 eV), directly linked to a downward trend in ionic conductivity. The presence of a less conductive phase, PEO_{10}:LiTFSI, located between Li_6PS_5Cl particles increases tortuosity within the highly conductive ceramic percolating network. As the organic phase content increases, the tortuosity increases, thus the lithium conduction becomes weaker. Here, we propose to use the activation mechanism fitting as an easily accessible metric to gain a deeper understanding of the HSE ionic pathway. These results support the hypothesis of Li^+ conduction *via* the organic matrix in HSEs with 20 to 60 wt.% of ceramic, while Li_6PS_5Cl particles may be the preferred pathway for lithium ions at higher ceramic contents (75 to 95 wt.%).

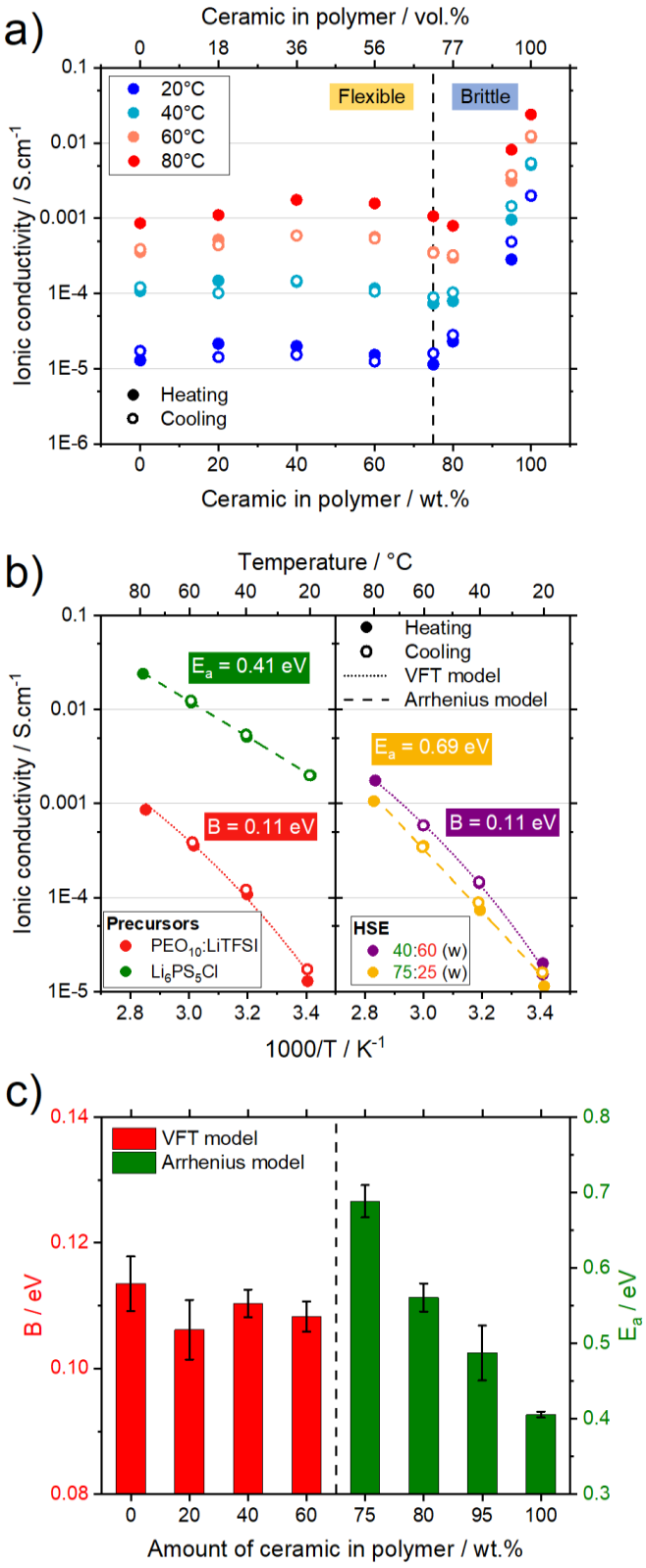

Figure 2: (a) HSE ionic conductivity according to organic-to-inorganic ratio and temperature, (b) activation mechanism for precursor and HSE, and (c) associated energies of Arrhenius and VFT models.

Polymer molar mass

Since conductivity and mechanical criteria cannot be met by simply adjusting the organic-to-inorganic ratio, we took advantage of the wide range of molar masses available for PEO to study the effect of reducing the polymer length on the ionic conductivity. Figure 3a shows the increase of conductivity in PEO_{10}:LiTFSI systems due to polymer shortening (from 600 to 0.4 $kg.mol^{-1}$), as previously observed by Devaux et al.[27] A lower molar mass decreases the glass transition and increases chain mobility due to a greater amount of end groups, which are more mobile than the backbone. The consequence is an increase of free volume and hence ionic conductivity[31]. Reducing the weight of PEO from 600 to 0.4 $kg.mol^{-1}$ results in a three-fold gain of the conductivity (from 1.5 ± 0.2 to 4.6 ± 0.4 · 10^{-5} $S.cm^{-1}$) at room temperature. The effect is significantly higher when we switch to a HSE system with high inorganic content (PEO_{10}:LiTFSI : Li_6PS_5Cl = 25:75 (w) – Fig. 3b). The benefit is in this case twelve-fold, from 1.4 ± 0.2 to 17 ± 4 · 10^{-5} $S.cm^{-1}$. This means that the addition of Li-conductive ceramic particles has a clear positive impact on the ionic mobility through the HSE, regardless of the initial conductivity of the organic phase. The quality of the mixing between the two precursor electrolytes may explain the difference between high and low molar mass systems. At room temperature, PEO_{10}:LiTFSI (600 $kg.mol^{-1}$) is in solid-state, requiring hot-processing (around 80°C) to mix it with Li_6PS_5Cl. In contrast, PEO_{10}:LiTFSI (0.4 $kg.mol^{-1}$) is in liquid-state at 25°C, making mixing easier and more complete (cross-section SEM images in Fig. S6). PEO chain length can also have an impact on the arrangement of ceramic particles within the organic matrix. The percolation of the inorganic phase is easier to access in a low molar mass system since the viscosity of the organic phase is lower[27], which explains the beneficial effect on ionic conductivity. While the conductivity criterion is met for the low molar mass PEO system (0.4 $kg.mol^{-1}$) with a conductivity over 10^{-4} $S.cm^{-1}$ at room temperature, this HSE suffers from poor mechanical properties as it is a brittle material that cannot be processed as a thin and flexible self-standing membrane (Fig. S6).

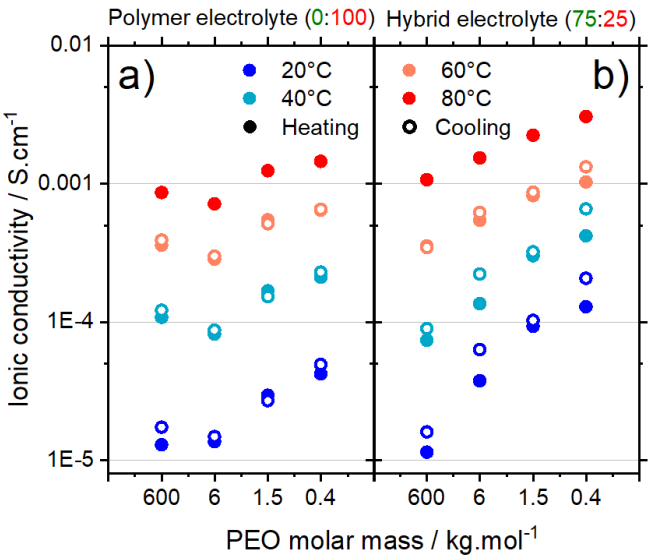

Figure 3: Temperature-dependent ionic conductivity of HSE (75 wt.% Li_6PS_5Cl – (b)) compared to polymer electrolyte (a) according to PEO molar mass.

Mixed molar masses HSE

Given that high molar mass PEO is known to enhance the elasticity of an electrolyte[38] and based on our findings that a low molar mass PEO (referred as PEG in the following text) allows a better mixing and therefore higher conductivity, the logical approach is to formulate a HSE based on an organic phase with mixed molar masses. To this end, a polymer electrolyte was prepared with PEO (600 $kg.mol^{-1}$) and PEG (0.4 $kg.mol^{-1}$) at different ratios (1:0, 2:1, 1:1, 1:2 and 0:1 (w)). They were mixed with 75 wt.% of Li_6PS_5Cl to obtain a range of high ceramic-loading HSEs; their ionic conductivities at temperature are shown in Figure 4a. As predicted from previous discussion, increasing amount of PEG improves the ionic conductivity at 20°C. Up to 50 wt.%, this benefit is significant with a five-fold increase (1.4 ± 0.2 to $7.7 \pm 0.9 \cdot 10^{-5}$ $S.cm^{-1}$). For higher amounts of PEG, the gain in conductivity is smaller (only twofold from 50 to 100 wt.%) and the loss of mechanical properties is too important to be interesting in terms of formulation. HSE with the polymer blend PEO:PEG=1:2 (w) is indeed a brittle material (Fig. S7). To finalize the formulation, the ceramic content was varied from 70 to 80 wt.% to check the influence on ionic conductivity and mechanical properties (Fig. S8). It was confirmed that a HSE with 75 wt.% of ceramic is the best compromise in terms of conductivity and mechanical properties. Figure 4b shows the ionic conductivities of the precursor materials and the HSEs as a function of temperature and their respective mechanisms. It appears that the HSE with the modified organic phase follows an Arrhenius law and has a higher activation energy (0.51

eV) compared with pure Li_6PS_5Cl (0.41 eV). Here, shifting from the initial PEO_{10}:LiTFSI to the modified $(PEO:PEG=1:1)_{10}$:LiTFSI polymeric matrix enables a significant reduction in activation energy from 0.69 to 0.51 eV. The conductivity criterion is reached here with 10^{-4} S.cm^{-1} at room temperature (25°C). The SEM cross-section (Fig. 4c) shows the overall homogeneity and the possibility of processing the optimized HSE as thin membranes (80 µm). This feature is essential to ensure low ohmic drop and high energy density in a complete cell configuration. As a point of comparison, a conductivity of $6 \cdot 10^{-5}$ S.cm^{-1} at 30°C was obtained by Simon et al.[20] using 40 wt.% of Li_6PS_5Cl and 60 wt.% of PEO_{20}:LiTFSI, which is close to our measurements (Fig. 2b). Following a similar solvent-based route, Li et al.[2] explored HSEs based on $Li_{10}GeP_2S_{12}$ (LGPS – $\sigma_{ion} = 10^{-2}$ S.cm^{-1}) and PEO_{10}:LiTFSI and obtained a maximum conductivity of was 10^{-5} S.cm^{-1} at 20°C with 90 wt.% of LGPS, indicating no synergy between the phases. Our systematic approach successfully reaches higher room temperature conductivity following a straightforward solvent-free process. In the transition to larger scale production of our HSE, the optimized mixture was processed as a membrane in a dry room (dew point below -40°C) using a calendering machine. It was observed that this operation systematically induced long cracks, preventing the preparation of large area HSE (Fig. S9a). To solve this problem, the homopolymer (PEO 600 kg.mol^{-1}) was replaced by a copolymer, known to be less resistant to creep and to have higher tensile strength. The chosen copolymer differs only in the presence of a propylene oxide unit at a 12:1 ratio with ethylene oxide units (Fig. S9b) and the new HSE exhibits similar ionic conductivity at room temperature ($0.9 \cdot 10^{-4}$ S.cm^{-1}), when prepared in the glovebox. It is referred to P(EO-co-PO) in the following discussion and has a similar molecular weight (average of 1000 kg.mol^{-1}). In the dry room, the preparation of large area membranes (around 30 cm^2) was possible without crack propagation from the edges (Fig. S9c). However, significant water uptake occurs during the manufacturing process (approximately 3000 ppm), rendering the HSE unsuitable for additional characterization due to probable degradation. Therefore, stricter control of water levels is necessary to avoid this constraining phenomenon. Nevertheless, we demonstrate the feasibility of preparing critical-size HSE membranes using a solvent-free process.

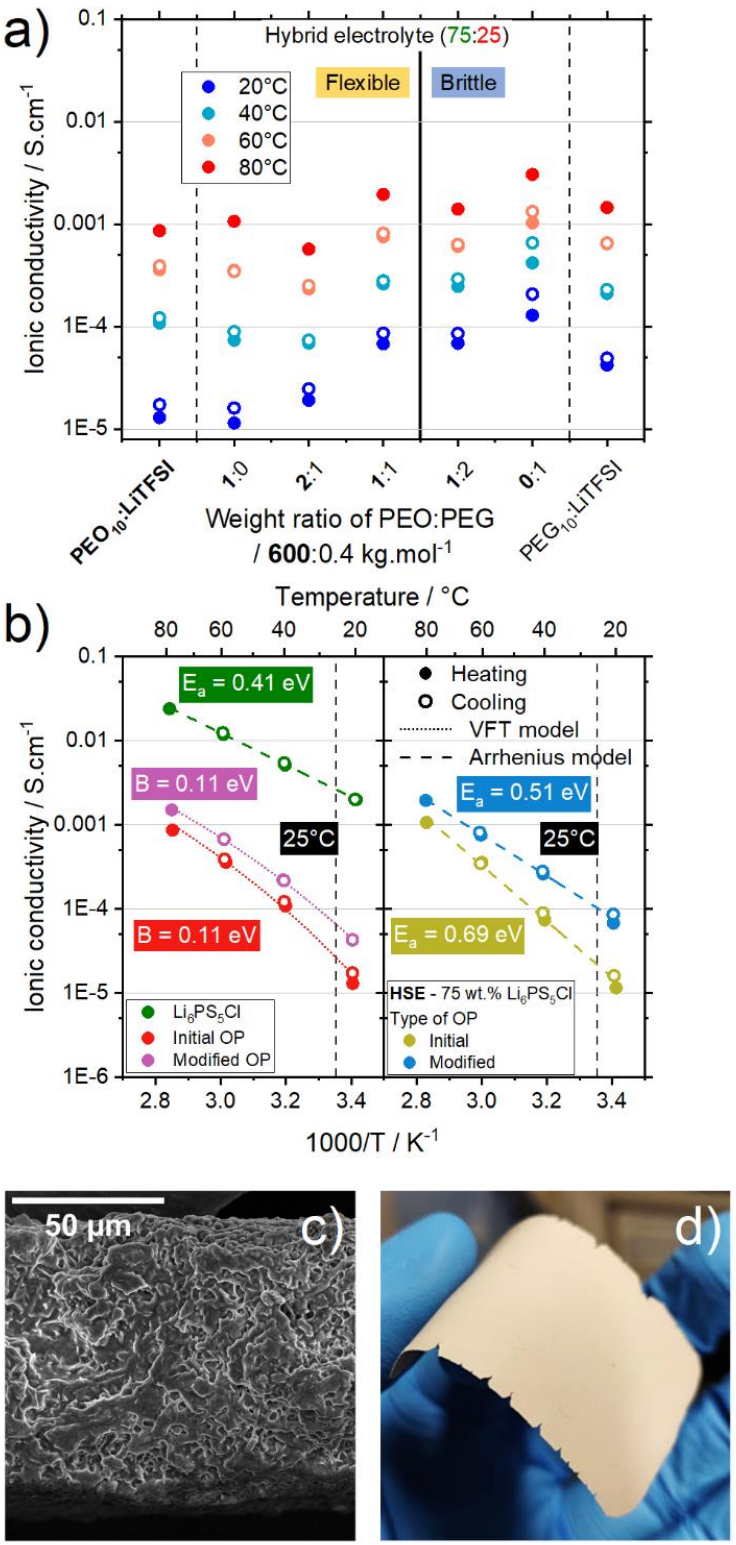

Figure 4: Combination of high and low molar mass PEO in high-loading ceramic HSE. (a) Effect of PEO:PEG ratio to HSE ionic conductivity in temperature. (b) Activation mechanism for precursors and 75 wt.% ceramic HSEs. Initial organic phase (OP): PEO_{10}:LiTFSI – Modified OP: $(PEO:PEG = 1:1\ (w))_{10}$:LiTFSI. (c) SEM picture of the optimized HSE cross-section. (d) Image of the large area optimized HSE membrane.

Mechanical characterization of HSE

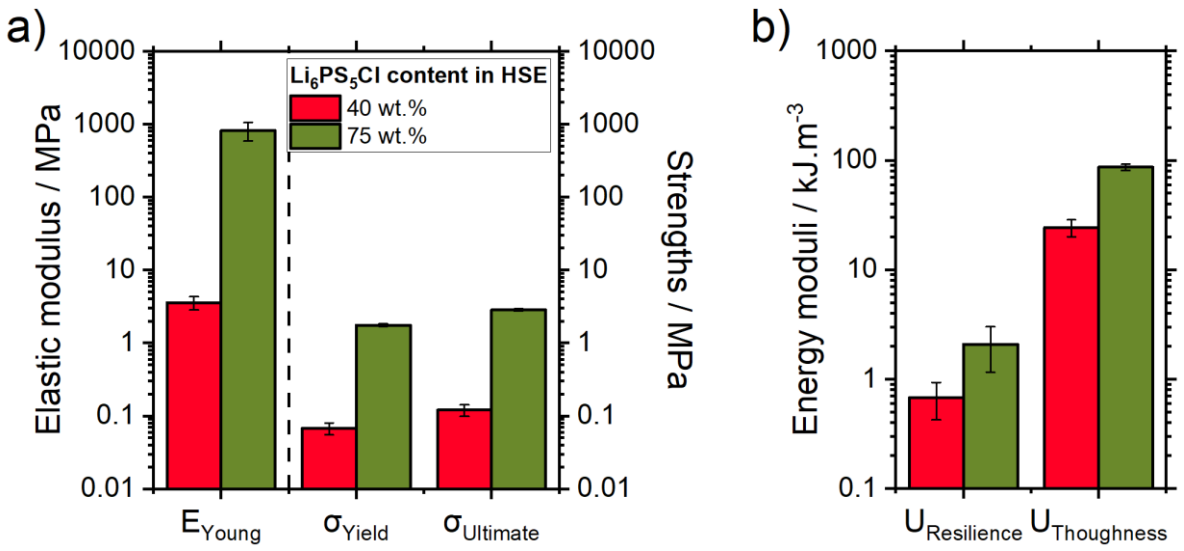

Figure 5: Evolution of HSE tensile properties with ceramic amount: (a) Young's modulus, yield and ultimate strengths, (b) resilience and toughness moduli.

To assess the difference in mechanical behavior between HSEs, a tensile test was performed on two representative membranes. Li_6PS_5Cl content was set to 40 and 75 wt.% to compare a *ceramic-in-polymer* system with a *polymer-in-ceramic* one. The organic phase was kept identical as the optimized one, $[P(EO\text{-}co\text{-}PO):PEG=1:1]_{10}$:LiTFSI. Figure S10 shows the stress-strain curves for HSE, demonstrating good reproducibility in both cases. It is another indication of the homogeneity of the dry mixing. Changing the organic-to-inorganic ratio leads to very different mechanical behaviors. Low ceramic-content HSE (40 wt.%) deforms mainly in a plastic regime (ε = 25%) under low applied stress (σ = 0.12MPa). This results in a low Young's modulus of 3.6 MPa (Fig. 5a), which is 200 times smaller than the high ceramic-content HSE (75 wt.%). The Young's modulus of 0.82 GPa illustrates the stronger elastic behavior of the optimized formulation. Overall, the *polymer-in-ceramic* configuration withstands higher stress under elastic (resp. plastic) deformation than the ceramic-in-polymer one – yield stress σ_y = 1.8 MPa (Fig. 5a) *versus* 0.067 MPa (resp. ultimate strength σ_u = 2.8 MPa *versus* 0.12 MPa). In terms of its ability to absorb mechanical energy, the high-ceramic content HSE still outperforms the low content one. The resilience modulus U_r (energy absorbed under elastic deformation i.e. reversible) is 2.1 $kJ.m^{-3}$ compared to 0.68 $kJ.m^{-3}$ (Fig. 5b). In the same trend, the toughness modulus U_t (energy absorbed before fracture i.e. non-reversible) is almost four

times higher (86.5 kJ.m^{-3} *versus* 24.3 kJ.m^{-3}). This tensile characterization demonstrates that the addition of Li_6PS_5Cl particles is beneficial for mechanical resistance of the HSE. To compare our results with other work, Lopez et al.[39] have characterized the tensile behavior of a PEO_{10}:LiTFSI membrane and found a Young's modulus of 0.4 MPa, which is much lower than our optimized HSE. The yield strength is also lower (σ_y = 0.04 MPa) as the material deforms mainly plastically under a long stress plateau. However, resilience (U_r = 3 kJ.m^{-3}) and toughness moduli (U_t = 40-50 kJ.m^{-3} – estimated graphically) are comparable. Although our HSE withstands a higher mechanical stress, this means that it is a more brittle material than the conventional polymer electrolyte, which may be expected given the high content of Li_6PS_5Cl, known to be a brittle ceramic. Ultimately, we show that a combined increase of ionic conductivity (σ_i = 10^{-5} to 10^{-4} S.cm^{-1} at 25°C) and mechanical resistance is possible using a systematic formulation approach for HSEs. Improving the mechanical properties of polymer or hybrid electrolytes generally leads to a drop in conductivity. Stolz et al.[28] demonstrated the negative correlation between compression resistance and ionic conductivity at 40°C by simply changing the salt concentration in PEO_x:LiTFSI (x = 10 – 50). Lee et al.[40] studied a HSE composed of PEO_{20}:LiTFSI and LAGP, and showed that increasing the ceramic amount has a positive impact on the Young's modulus, although it strongly affects the toughness and the ionic conductivity.

Chemical compatibility of phases

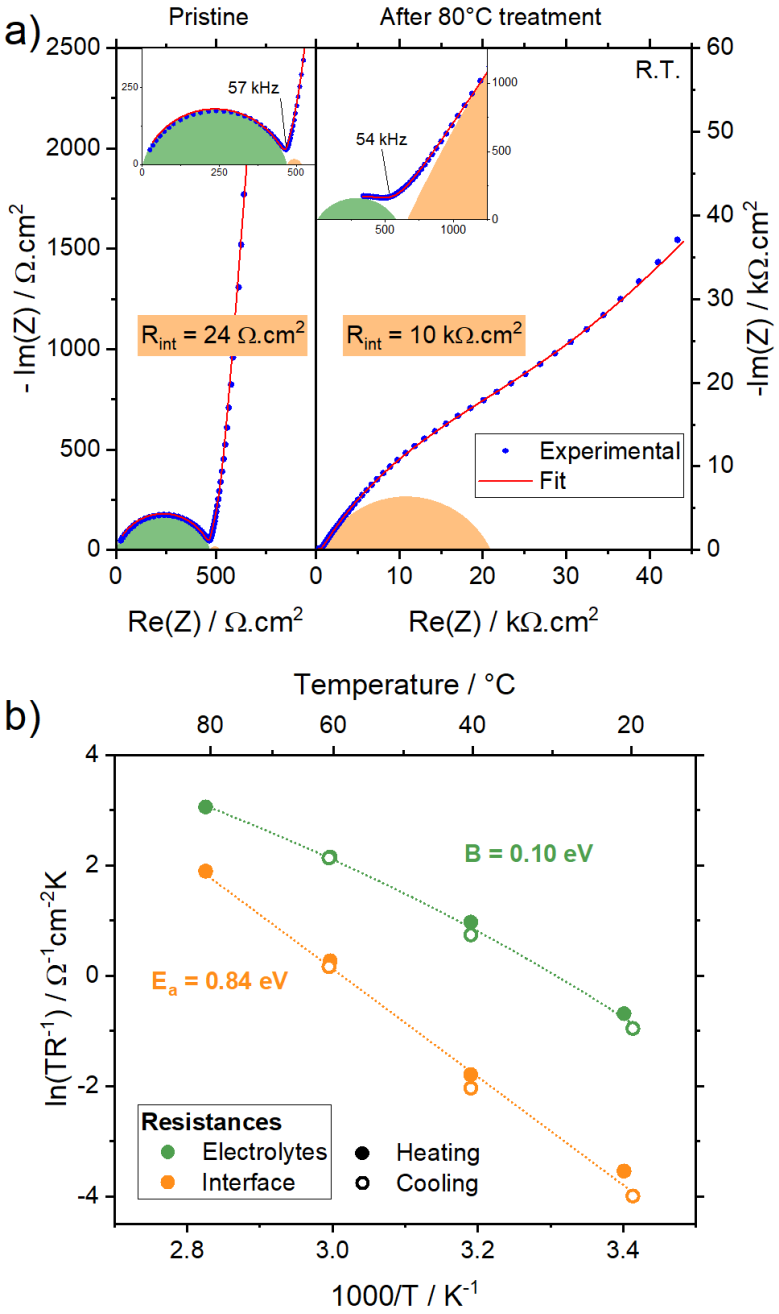

Figure 6: Compatibility of ceramic and polymer phases probed by EIS. (a) EIS spectra of trilayer PEO_{10}:LiTFSI | Li_6PS_5Cl | PEO_{10}:LiTFSI before and after 80°C treatment. (b) Evolution of R_{elec} and R_{int} in temperature and their related activation energies.

In addition to sufficient ionic conductivity and mechanical properties, compatibility between organic and inorganic phases is another essential parameter for HSE to quantify. X-ray photoelectron spectroscopy (XPS) was first performed on a HSE containing 40 wt.% of Li_6PS_5Cl and after a thermal aging treatment for six days at 80°C. Comparison of the S2p spectra shows

a direct impact of temperature on the stability of the ceramic in contact with the polymer phase (Fig. S11a-d). Degraded sulfide species are formed with the appearance of a polysulfide peak. However, in comparison to the work of Simon et al.[20], dry mixing of the precursors seems less detrimental to the chemical stability of HSE than the slurry route using THF. In our study, no polysulfide or other degradation species can be identified in the S2p spectrum of pristine HSE. Nor is there any evidence of LiF formation on the HSE F1s spectrum (Fig. S11e-g), even after the aging procedure, in the absence of solvent. This demonstrates the value of avoiding solvents when formulating HSE. Since XPS measurements revealed the impact of temperature on the chemical stability of HSE, an EIS study from 20 to 80°C was carried out to quantify the interfacial resistance between organic and inorganic phases. Trilayer stacks of PEO_x:LiTFSI | Li_6PS_5Cl | PEO_x:LiTFSI (x = 10, 20 and 40) were assembled with blocking electrodes at a low pressure of 4.5 MPa in order to prevent polymer creep around the ceramic pellet or along the stainless steel pistons. Impedance contributions were assigned by varying the salt concentration, i.e. the polymer electrolyte ionic conductivity (Fig. S12). The high frequency semi-circle describes the electrolytes conduction (picofarad range) while the interfacial contribution appears at medium frequencies (nanofarad range), both of which increase with decreasing salt concentration. Figure 6a shows the unambiguous growth of the interfacial resistance after one hour treatment at 80°C for the x = 10 system, while the semi-circle attributed to the electrolyte conduction of the trilayer remains stable. Figure 6b shows the temperature-dependence of the electrolytes and interface resistances after performing the heat treatment displayed in Figure 6a. It shows the stability of the values during the measurements and equilibration time (around 22h in total) as the heating and cooling data match well. Electrolytes resistance follows a VFT model, confirming that polymer electrolyte layers are the limiting conduction step, since they have a lower conductivity (2.10^{-5} $S.cm^{-1}$) than ceramic at low pressure (4.10^{-4} $S.cm^{-1}$). Figure S13 shows the significant effect of lowering the pressure on the conductivity of a Li_6PS_5Cl pellet, probably due to loss of mechanical cohesion between the particles. Considering the interfacial resistance (Fig. 6b), it follows an Arrhenius law with a high activation energy of 0.84 eV. Assuming the formation of an interphase between the organic and inorganic phases (see NMR section for supporting this hypothesis), this is an energetically unfavorable obstacle to the passage of Li ions, since its activation energy is much higher than that of the pure ceramic phase (0.44 eV – Fig. S13). This result is in reasonable agreement with the reported value of 0.67 eV[41], where the author used

a more accurate setup with four-point EIS measurement. Overall, we have identified the negative effect of high temperature on the chemical stability of our HSE via the formation of interphases with high activation energies, hence the need for a room temperature processing.

NMR characterization of interphase formation

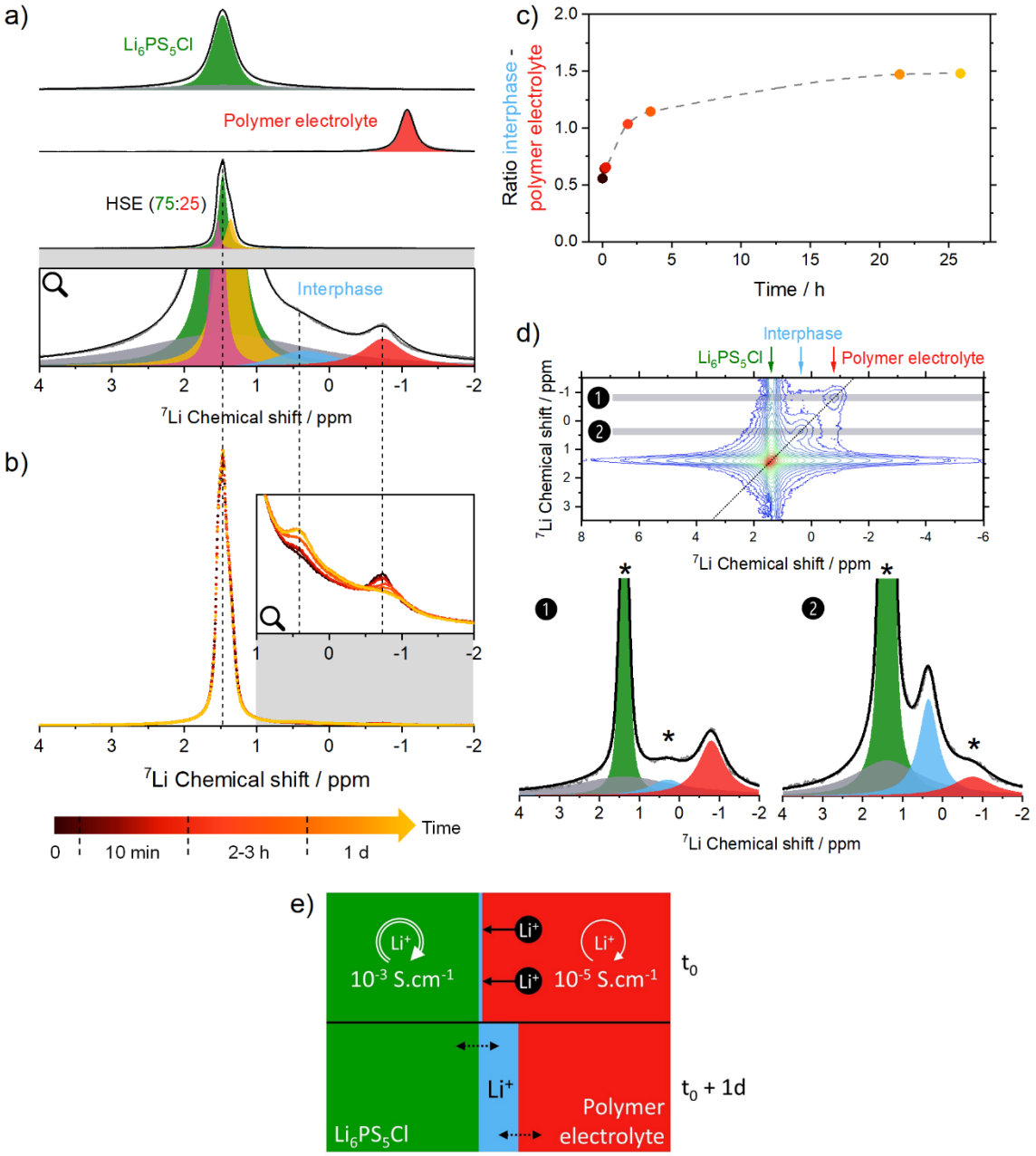

Figure 7: (a) ^{7}Li MAS NMR spectra of precursors phases (Li_6PS_5Cl and P(EO-co-PO):PEG:LiTFSI) and optimized HSE (75 wt.% ceramic). The experimental spectrum is shown in grey and the model in black. (b) ^{7}Li MAS NMR spectrum of HSE as a function of time. (c) Ratio of interphase and organic phase intensities as a function of time. Grey dashed line acts as a visual guide. (d) 2D ^{7}Li EXchange SpectroscopY (EXSY) spectrum obtained for optimized HSE. 1D ^{7}Li spectra are

obtained from the sum of 0.234 ppm wide slices to identified off-diagonal peaks (*). (e) Schematics of the interphase formation via the depletion of the organic phase.

To better understand the structural environments of lithium in our HSE, we used solid-state ^{7}Li Magic Angle Spinning NMR. Reference spectra of Li_6PS_5Cl and polymer electrolyte (P(EO-co-PO):PEG:LiTFSI) facilitate identification of contributions in the spectrum of our optimized HSE (75 wt.% ceramic) (Fig. 7a). Two components centered on 1.47 ppm are observed in the pure ceramic spectrum accounting for 67.9% (green and sharp) and 32.1% (grey and broad). Several factors can explain the presence of two components: firstly, ^{7}Li ions are quadrupolar (nuclear spin S = 3/2) and quadrupolar relaxation is intrinsically biexponential, especially for samples where the correlation time of the environment fluctuations (i.e. site-to-site jumps) is close to the inverse of the Larmor frequency (3 ns for 330 MHz here). In such a case, biexponential relaxation leads to a complex line shape which is made of two Lorentzian lines, a broad one representing 60% of the signal and a narrower one accounting for the remaining 40%.[42] This applies to a homogeneous sample, and in this case, heterogeneities (magnetic field inhomogeneities, interfaces, defects, differences in lithium mobility) may lead to additional sources of broadening that will lead to a more complex line shape. The overall heterogeneity of the sample in terms of particle size (1 – 30 μm; Fig. S2) may be one of the reason for this phenomenon. The spectrum acquired with the pure polymer electrolyte displays a single component at -1.07 ppm (red). When the organic phase is mixed with Li_6PS_5Cl, the resonance from Li^+ in LiTFSI shifts to -0.74 ppm and the peak broadens. This indicates a change in the local Li^+ environment in the polymer phase. Indeed, most of the volume in the HSE is occupied by ceramic particles (72 vol.%), which alters the global susceptibility and magnetic field experienced by the organic phase. The peak accounts for 2.15% of the signal, as described by the model (Fig. S14a) in line with the theoretical calculation giving 2.0% of the overall lithium in the organic phase (see Experimental section for calculation). There is also a change in the Li_6PS_5Cl peak which becomes asymmetric, with two additional contributions at 1.53 ppm (pink) and 1.36 ppm (yellow). This is again the signature of a global disorder within the hybrid sample, and of a possible discontinuity in magnetic susceptibilities at the interface between the organic and the inorganic phases. A new feature appears at 0.33 ppm (blue), as a right shoulder to the ceramic resonance. Its position between the ceramic and the polymer environments suggests that this is the interphase, the existence of which was previously

deduced by EIS analysis. The HSE was prepared just before the measurement, enabling us to follow the appearance of this peak over time as shown in Figure 7b. It is interesting to note that the increase and the sharpening of the interphase peak are simultaneous with the decrease in the contribution of the polymer electrolyte, confirming the nature of this new, less mobile lithium environment for lithium. Lithium from the polymer phase gets trapped in the interphase created by a slow chemical reaction. Quantitative analysis of spectra, acquired at different times from a few minutes to one day after mixing, enables the intensity of each contribution to be calculated (Fig. S14h). To support the observed evolution of the peaks, the intensity ratio between the interphase and the organic phase was calculated (Fig. 7c). It shows a rapid increase from 0.5 to 1.0 within the first three hours, followed by a slower increase up to 1.5 and stabilization after one day. This highlights a phenomenon of lithium depletion in the organic phase to form the interphase, which tends to stabilize after one day.

To probe the exchange ability of lithium between phases, a homonuclear 2D Exchange SpectroscopY (EXSY, see Fig. 7d) was performed with a 100 ms mixing delay under ultra-fast Magic Angle Spinning (40 kHz) to quench spin diffusion resulting from weak dipolar interactions. As two ^{7}Li spins separated by 3 Å experience a dipolar interaction of 672 Hz in magnitude, we considered that spin diffusion is negligible at such a fast MAS rate, and that lithium should be further apart, particularly in the polymer phase. In the resulting contour plot, the intense and broad cross region is the signature of the disordered Li_6PS_5Cl environment. Less intense peaks are identified on the diagonal as the interphase and polymer electrolyte environments. Off-diagonal intensity is detected between the interphase, ceramic and organic phase environments. To clearly observe the chemical exchange process, we analyzed the 1D cross sections (grey areas) centered on the organic (1) and interphase (2) environments. Both reveal chemical exchange between the interphase, the organic electrolyte and the ceramic phase. Despite the resistive nature of the interphase, previously observed by EIS, this confirms that lithium ions slowly diffuse across the interphase over a 100 ms timescale. However, evidence of Li exchange at the micrometric scale is not necessarily synonymous with macroscopic Li conduction through both phases, as we have previously elucidated through conductivity measurements and activation mechanisms.

Electrochemical performances of the HSE

From a practical perspective, our optimized HSE has been tested in a NMC:Li_6PS_5Cl:VGCF:PVDF-HFP | HSE | $Li_{0.5}In$:Li_6PS_5Cl solid-state battery to assess its electrochemical performances. It is compared with our reference Li_6PS_5Cl-based separator for SSB, both cycling at 100 MPa in airtight cells at room temperature, to ensure sufficient contact between all components and prevent any moisture-induced degradation (Fig. S15). Here, an in-house prepared cathode tape is used to ensure good reproducibility between cells. Figure 8a shows the first cycle voltage profile at C/20, which reveals a higher polarization when employing HSE as a solid-state separator instead of a densified ceramic pellet, despite a lower cathode mass loading. The result is a discharge capacity 15% lower for the HSE battery (130.2 $mAh.g^{-1}$) than for the reference batteries (153.25 $mAh.g^{-1}$). This figure is nonetheless encouraging as the thinner hybrid membrane (87 µm) compared with the Li_6PS_5Cl separator (≈ 400 µm) does not compensate for the lower ionic conductivity of the HSE (10^{-4} $S.cm^{-1}$ *versus* $3 \cdot 10^{-3}$ $S.cm^{-1}$). However, as the ohmic drop becomes significant at a higher C-rate (Fig. 8b), polarization increases more rapidly for the HSE battery than for the reference battery, resulting in almost zero capacity at 1C. When the current density is reduced to C/5 (Fig. 8c), both systems return to their previous capacity levels and show good capacity retention, with a similar decay rate of -0.14 $mAh.g^{-1}.cycle^{-1}$ (resp. -0.155) for the HSE-based battery (resp. pure ceramic batteries). Finally, these data indicate that it is possible to operate a battery assembled with our optimized HSE, with low capacity loss at a slow C-rate. However, the insufficient ionic conductivity of the HSE compared with the Li_6PS_5Cl separator affects the capacity accessible at higher C-rates due to greater polarization. More interestingly, the capacity retention at C/5 is not affected by replacing the pure ceramic separator with the HSE. A possible strategy to overcome the poor performances at higher C-rates, or similarly at higher cathode loads, could be to reduce the HSE thickness to less than 10 µm to have an ohmic drop equivalent to that of the reference battery. For the time being, this prospect is limited by the size of Li_6PS_5Cl particles, some of which exceed 30 µm. On the other hand, the interfaces at the cathode and anode may not be as optimized with the HSE as with pure ceramic, which would require some surface engineering (use of temperature, roll-to-roll assembly).

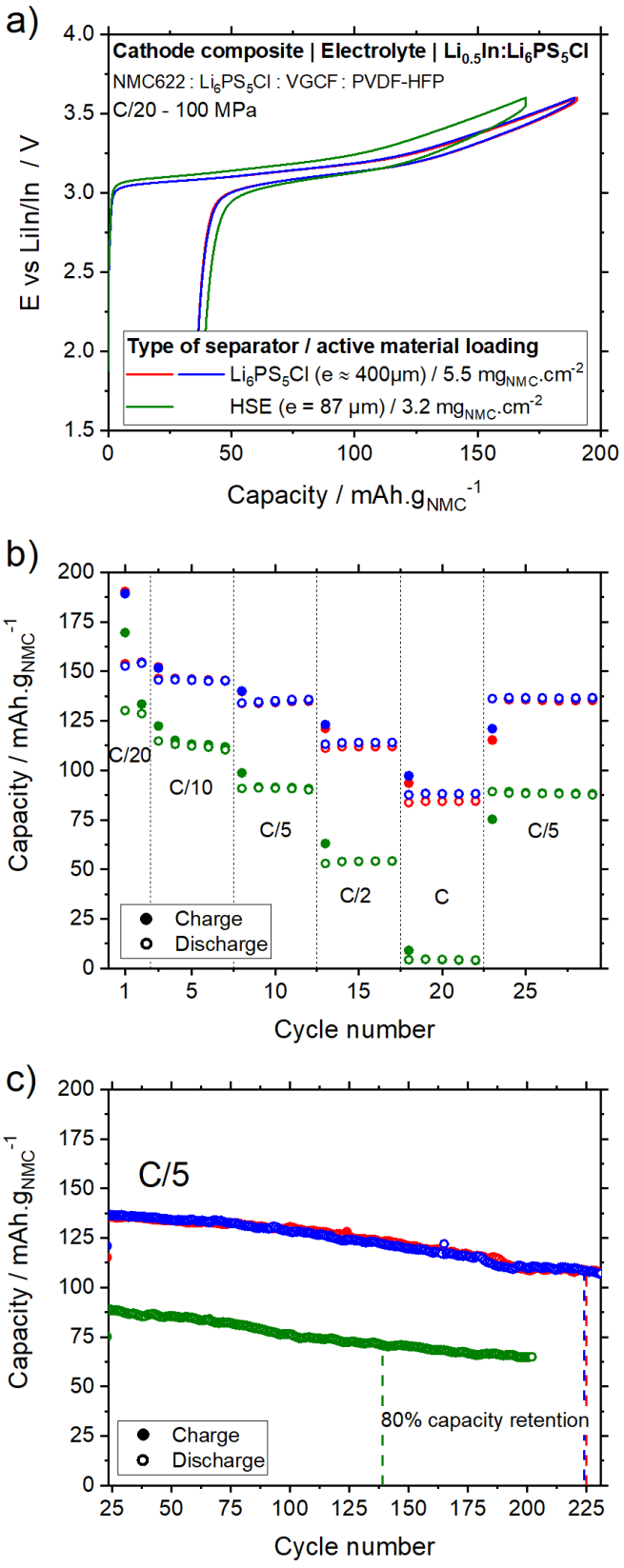

Figure 8: Electrochemical performances of a HSE-based battery. Comparison between batteries based on HSE (1 cell) or pure Li_6PS_5Cl separator (2 cells): (a) first cycle voltage profile. (b) C-rate behavior and (c) capacity retention at C/5.

CONCLUSION

In this study, our aim was to develop a hybrid solid electrolyte (HSE) with good ionic conductivity (10^{-4} S.cm^{-1} at 25°C) and mechanical properties. We used PEO_{10}:LiTFSI and Li_6PS_5Cl as the organic and inorganic components and employed a solvent-free method to prepare the HSE, preventing ceramic degradation. The addition of Li_6PS_5Cl improved ionic conductivity beyond 75 wt.%, but it compromised mechanical strength, representing a typical trade-off in HSEs. To address it, we reduced PEO molar mass and proposed a modified organic matrix that combines elasticity and ionic conductivity, resulting in a high-ceramic loading HSE that meets our criteria. Additionally, we introduced a novel approach by utilizing activation mechanism fitting as a powerful metric to elucidate the preferred ionic pathway within HSEs. The VFT model serves as a signature of organic conductivity, while the Arrhenius model characterizes ceramic conductivity. Intrinsic chemical reactivity was investigated with EIS, which revealed temperature impact on interfacial resistance, and NMR, that confirmed the interphase growth. We evaluated the HSE membrane as a separator in batteries, showing decent cyclability at low C-rates and low cathode loading. However, its higher ohmic drop coming from lower conductivity affected high current densities cycling. Nevertheless, capacity retention remained comparable to that of pure-ceramic batteries, suggesting good stability with the electrodes. This study underscores the prime importance of optimizing ionic conductivity and mechanical properties concurrently, for successful HSE formulation, and provides valuable insights into key conduction mechanisms. Future research should focus on reducing membrane thickness through particle size control and limiting chemical reactivity, by polymer end group modification[43] or particle protective coating[44], to match pure ceramic battery performances. Ultimately, we hope this work serves as guideline for HSEs rational formulation, with emphasis on metric optimization driving further advancements.

ASSOCIATED CONTENT

The Supporting Information is available free of charge on the ACS Publications.

Choice of EO:Li ratio (ionic conductivity and DSC), SEM of Li_6PS_5Cl particles and various HSEs, fitting of the activation mechanisms, impedance of salt-free HSE, shift from homopolymer to copolymer (pictures), stress-strain curves of HSEs, XPS results on HSEs, EIS measurement on

trilayer stack varying EO:Li, effect of pressure on Li_6PS_5Cl ionic conductivity, NMR fitting of HSE, schematics of the electrochemical cells.

AUTHOR INFORMATION

Corresponding Author

E-mail: christel.laberty@sorbonne-universite.fr

ORCID

Christel Laberty-Robert: 0000-0003-3230-3164

Notes

The authors declare no competing financial interest.

ACKNOWLEDGMENTS

Financial support from BlueSolutions and the IR INFRANALYTICS FR2054 for conducting the research is gratefully acknowledged.

REFERENCES

(1) Janek, J.; Zeier, W. G. A Solid Future for Battery Development. *Nat Energy* **2016**, *1* (9), 16141. https://doi.org/10.1038/nenergy.2016.141.
(2) Kamaya, N.; Homma, K.; Yamakawa, Y.; Hirayama, M.; Kanno, R.; Yonemura, M.; Kamiyama, T.; Kato, Y.; Hama, S.; Kawamoto, K.; Mitsui, A. A Lithium Superionic Conductor. *Nature Mater* **2011**, *10* (9), 682–686. https://doi.org/10.1038/nmat3066.
(3) Abakumov, A. M.; Fedotov, S. S.; Antipov, E. V.; Tarascon, J.-M. Solid State Chemistry for Developing Better Metal-Ion Batteries. *Nat Commun* **2020**, *11* (1), 4976. https://doi.org/10.1038/s41467-020-18736-7.
(4) Doux, J.-M.; Yang, Y.; Tan, D. H. S.; Nguyen, H.; Wu, E. A.; Wang, X.; Banerjee, A.; Meng, Y. S. Pressure Effects on Sulfide Electrolytes for All Solid-State Batteries. *J. Mater. Chem. A* **2020**, *8* (10), 5049–5055. https://doi.org/10.1039/C9TA12889A.
(5) Xue, Z.; He, D.; Xie, X. Poly(Ethylene Oxide)-Based Electrolytes for Lithium-Ion Batteries. *J. Mater. Chem. A* **2015**, *3* (38), 19218–19253. https://doi.org/10.1039/C5TA03471J.
(6) Fenton, D. E.; Parker, J. M.; Wright, P. V. Complexes of Alkali Metal Ions with Poly(Ethylene Oxide). *Polymer* **1973**, *14* (11), 589. https://doi.org/10.1016/0032-3861(73)90146-8.
(7) Armand, M.; Duclot, M. Nouveaux matériaux élastomères à conduction ionique. 7832976, June 20, 1980.
(8) *Technologie de batteries - Bollore - Blue Solutions*. https://www.blue-solutions.com/technologie-de-batteries/ (accessed 2023-03-15).
(9) Teyssot, A. Etude de l'interface lithium métal / électrolyte polymère fondu ou gélifié. phdthesis, Ecole Polytechnique X, 2005. https://pastel.archives-ouvertes.fr/pastel-00001112 (accessed 2021-05-31).
(10) Croce, F.; Persi, L.; Scrosati, B.; Serraino-Fiory, F.; Plichta, E.; Hendrickson, M. A. Role of the Ceramic Fillers in Enhancing the Transport Properties of Composite Polymer Electrolytes. *Electrochimica Acta* **2001**, *46* (16), 2457–2461. https://doi.org/10.1016/S0013-4686(01)00458-3.

(11) Scrosati, B.; Croce, F.; Persi, L. Impedance Spectroscopy Study of PEO-Based Nanocomposite Polymer Electrolytes. *J. Electrochem. Soc.* **2000**, *147* (5), 1718. https://doi.org/10.1149/1.1393423.
(12) Adebahr, J.; Byrne, N.; Forsyth, M.; MacFarlane, D. R.; Jacobsson, P. Enhancement of Ion Dynamics in PMMA-Based Gels with Addition of TiO2 Nano-Particles. *Electrochimica Acta* **2003**, *48* (14–16), 2099–2103. https://doi.org/10.1016/S0013-4686(03)00191-9.
(13) Zheng, J.; Tang, M.; Hu, Y. Lithium Ion Pathway within $Li_7La_3Zr_2O_{12}$ -Polyethylene Oxide Composite Electrolytes. *Angew. Chem. Int. Ed.* **2016**, *55* (40), 12538–12542. https://doi.org/10.1002/anie.201607539.
(14) Gupta, A.; Sakamoto, J. Controlling Ionic Transport through the PEO-LiTFSI/LLZTO Interface. *Electrochem. Soc. Interface* **2019**, *28* (2), 63–69. https://doi.org/10.1149/2.F06192if.
(15) Zheng, J.; Hu, Y.-Y. New Insights into the Compositional Dependence of Li-Ion Transport in Polymer–Ceramic Composite Electrolytes. *ACS Appl. Mater. Interfaces* **2018**, *10* (4), 4113–4120. https://doi.org/10.1021/acsami.7b17301.
(16) Zheng, J.; Wang, P.; Liu, H.; Hu, Y.-Y. Interface-Enabled Ion Conduction in $Li_{10}GeP_2S_{12}$ –Poly(Ethylene Oxide) Hybrid Electrolytes. *ACS Appl. Energy Mater.* **2019**, *2* (2), 1452–1459. https://doi.org/10.1021/acsaem.8b02008.
(17) Li, M.; Kolek, M.; Frerichs, J. E.; Sun, W.; Hou, X.; Hansen, M. R.; Winter, M.; Bieker, P. Investigation of Polymer/Ceramic Composite Solid Electrolyte System: The Case of PEO/LGPS Composite Electrolytes. *ACS Sustainable Chem. Eng.* **2021**, *9* (34), 11314–11322. https://doi.org/10.1021/acssuschemeng.1c00904.
(18) Chen, S.; Wang, J.; Zhang, Z.; Wu, L.; Yao, L.; Wei, Z.; Deng, Y.; Xie, D.; Yao, X.; Xu, X. In-Situ Preparation of Poly(Ethylene Oxide)/Li3PS4 Hybrid Polymer Electrolyte with Good Nanofiller Distribution for Rechargeable Solid-State Lithium Batteries. *Journal of Power Sources* **2018**, *387*, 72–80. https://doi.org/10.1016/j.jpowsour.2018.03.016.
(19) Li, D.; Cao, L.; Liu, C.; Cao, G.; Hu, J.; Chen, J.; Shao, G. A Designer Fast Li-Ion Conductor Li6.25PS5.25Cl0.75 and Its Contribution to the Polyethylene Oxide Based Electrolyte. *Applied Surface Science* **2019**, *493*, 1326–1333. https://doi.org/10.1016/j.apsusc.2019.07.041.
(20) Simon, F. J.; Hanauer, M.; Richter, F. H.; Janek, J. Interphase Formation of PEO_{20}:LiTFSI–Li_6PS_5Cl Composite Electrolytes with Lithium Metal. *ACS Appl. Mater. Interfaces* **2020**, *12* (10), 11713–11723. https://doi.org/10.1021/acsami.9b22968.
(21) Chen, L.; Li, Y.; Li, S.-P.; Fan, L.-Z.; Nan, C.-W.; Goodenough, J. B. PEO/Garnet Composite Electrolytes for Solid-State Lithium Batteries: From "Ceramic-in-Polymer" to "Polymer-in-Ceramic." *Nano Energy* **2018**, *46*, 176–184. https://doi.org/10.1016/j.nanoen.2017.12.037.
(22) Horowitz, Y.; Lifshitz, M.; Greenbaum, A.; Feldman, Y.; Greenbaum, S.; Sokolov, A. P.; Golodnitsky, D. Review—Polymer/Ceramic Interface Barriers: The Fundamental Challenge for Advancing Composite Solid Electrolytes for Li-Ion Batteries. *J. Electrochem. Soc.* **2020**, *167* (16), 160514. https://doi.org/10.1149/1945-7111/abcd12.
(23) Ruhl, J.; Riegger, L. M.; Ghidiu, M.; Zeier, W. G. Impact of Solvent Treatment of the Superionic Argyrodite Li6PS5Cl on Solid-State Battery Performance. *Advanced Energy and Sustainability Research* **2021**, *2* (2), 2000077. https://doi.org/10.1002/aesr.202000077.
(24) Tan, D. H. S.; Banerjee, A.; Deng, Z.; Wu, E. A.; Nguyen, H.; Doux, J.-M.; Wang, X.; Cheng, J.; Ong, S. P.; Meng, Y. S.; Chen, Z. Enabling Thin and Flexible Solid-State Composite Electrolytes by the Scalable Solution Process. *ACS Appl. Energy Mater.* **2019**, *2* (9), 6542–6550. https://doi.org/10.1021/acsaem.9b01111.

(25) Ludwig, B.; Zheng, Z.; Shou, W.; Wang, Y.; Pan, H. Solvent-Free Manufacturing of Electrodes for Lithium-Ion Batteries. *Sci Rep* **2016**, *6* (1), 23150. https://doi.org/10.1038/srep23150.
(26) Lu, Y.; Zhao, C.-Z.; Yuan, H.; Hu, J.-K.; Huang, J.-Q.; Zhang, Q. Dry Electrode Technology, the Rising Star in Solid-State Battery Industrialization. *Matter* **2022**, *5* (3), 876–898. https://doi.org/10.1016/j.matt.2022.01.011.
(27) Devaux, D.; Bouchet, R.; Glé, D.; Denoyel, R. Mechanism of Ion Transport in PEO/LiTFSI Complexes: Effect of Temperature, Molecular Weight and End Groups. *Solid State Ionics* **2012**, *227*, 119–127. https://doi.org/10.1016/j.ssi.2012.09.020.
(28) Stolz, L.; Röser, S.; Homann, G.; Winter, M.; Kasnatscheew, J. Pragmatic Approaches to Correlate between the Physicochemical Properties of a Linear Poly(Ethylene Oxide)-Based Solid Polymer Electrolyte and the Performance in a High-Voltage Li-Metal Battery. *J. Phys. Chem. C* **2021**, acs.jpcc.1c03614. https://doi.org/10.1021/acs.jpcc.1c03614.
(29) Marzantowicz, M.; Dygas, J. R.; Krok, F.; Nowiński, J. L.; Tomaszewska, A.; Florjańczyk, Z.; Zygadło-Monikowska, E. Crystalline Phases, Morphology and Conductivity of PEO:LiTFSI Electrolytes in the Eutectic Region. *Journal of Power Sources* **2006**, *159* (1), 420–430. https://doi.org/10.1016/j.jpowsour.2006.02.044.
(30) Marzantowicz, M.; Krok, F.; Dygas, J. R.; Florjańczyk, Z.; Zygadło-Monikowska, E. The Influence of Phase Segregation on Properties of Semicrystalline PEO:LiTFSI Electrolytes. *Solid State Ionics* **2008**, *179* (27–32), 1670–1678. https://doi.org/10.1016/j.ssi.2007.11.035.
(31) Ratner, M. A.; Shriver, D. F. Ion Transport in Solvent-Free Polymers. *Chem. Rev.* **1988**, *88* (1), 109–124. https://doi.org/10.1021/cr00083a006.
(32) Hanghofer, I.; Brinek, M.; Eisbacher, S. L.; Bitschnau, B.; Volck, M.; Hennige, V.; Hanzu, I.; Rettenwander, D.; Wilkening, H. M. R. Substitutional Disorder: Structure and Ion Dynamics of the Argyrodites Li_6PS_5Cl, Li_6PS_5Br and Li_6PS_5I. *Phys. Chem. Chem. Phys.* **2019**, *21* (16), 8489–8507. https://doi.org/10.1039/C9CP00664H.
(33) Vogel, D. H. Das Temperaturabhaengigkeitsgesetz Der Viskositaet von Fluessigkeiten. *Phys. Z.* **1921**, *22*, 645.
(34) Fulcher, G. S. Analysis of recent measurements of the viscosity of glasses. *J American Ceramic Society* **1925**, *8* (6), 339–355. https://doi.org/10.1111/j.1151-2916.1925.tb16731.x.
(35) Tammann, G.; Hesse, W. Die Abhängigkeit der Viscosität von der Temperatur bie unterkühlten Flüssigkeiten. *Z. Anorg. Allg. Chem.* **1926**, *156* (1), 245–257. https://doi.org/10.1002/zaac.19261560121.
(36) MacCallum, J. R.; Vincent, C. A. *Polymer Electrolyte Reviews*; Springer Science & Business Media, 1989.
(37) Roman, H. E. A Continuum Percolation Model for Dispersed Ionic Conductors. *J. Phys.: Condens. Matter* **1990**, *2* (17), 3909–3917. https://doi.org/10.1088/0953-8984/2/17/002.
(38) Jee, A.-Y.; Lee, H.; Lee, Y.; Lee, M. Determination of the Elastic Modulus of Poly(Ethylene Oxide) Using a Photoisomerizing Dye. *Chemical Physics* **2013**, *422*, 246–250. https://doi.org/10.1016/j.chemphys.2012.12.028.
(39) Lopez, J.; Sun, Y.; Mackanic, D. G.; Lee, M.; Foudeh, A. M.; Song, M.; Cui, Y.; Bao, Z. A Dual-Crosslinking Design for Resilient Lithium-Ion Conductors. *Adv. Mater.* **2018**, *30* (43), 1804142. https://doi.org/10.1002/adma.201804142.
(40) Lee, J.; Howell, T.; Rottmayer, M.; Boeckl, J.; Huang, H. Free-Standing PEO/LiTFSI/LAGP Composite Electrolyte Membranes for Applications to Flexible Solid-State Lithium-Based Batteries. *J. Electrochem. Soc.* **2019**, *166* (2), A416–A422. https://doi.org/10.1149/2.1321902jes.

(41) Simon, F. J.; Hanauer, M.; Henss, A.; Richter, F. H.; Janek, J. Properties of the Interphase Formed between Argyrodite-Type Li $_6$ PS $_5$ Cl and Polymer-Based PEO $_{10}$:LiTFSI. *ACS Appl. Mater. Interfaces* **2019**, *11* (45), 42186–42196. https://doi.org/10.1021/acsami.9b14506.
(42) Huynh, T. V.; Messinger, R. J.; Sarou-Kanian, V.; Fayon, F.; Bouchet, R.; Deschamps, M. Restricted Lithium Ion Dynamics in PEO-Based Block Copolymer Electrolytes Measured by High-Field Nuclear Magnetic Resonance Relaxation. *The Journal of Chemical Physics* **2017**, *147* (13), 134902. https://doi.org/10.1063/1.4993614.
(43) Huo, H.; Jiang, M.; Mogwitz, B.; Sann, J.; Yusim, Y.; Zuo, T.; Moryson, Y.; Minnmann, P.; Richter, F. H.; Veer Singh, C.; Janek, J. Interface Design Enabling Stable Polymer/Thiophosphate Electrolyte Separators for Dendrite-Free Lithium Metal Batteries. *Angew Chem Int Ed* **2023**, *62* (14). https://doi.org/10.1002/anie.202218044.
(44) Zhang, X.; Li, X.; Weng, S.; Wu, S.; Liu, Q.; Cao, M.; Li, Y.; Wang, Z.; Zhu, L.; Xiao, R.; Su, D.; Yu, X.; Li, H.; Chen, L.; Wang, Z.; Wang, X. Spontaneous Gas–Solid Reaction on Sulfide Electrolytes for High-Performance All-Solid-State Batteries. *Energy Environ. Sci.* **2023**, *16* (3), 1091–1099. https://doi.org/10.1039/D2EE03358E.

FOR TABLE OF CONTENT ONLY